A novel MYCN-specific antigene oligonucleotide deregulates mitochondria and inhibits tumor growth in MYCN-amplified neuroblastoma

A novel MYCN-specific antigene oligonucleotide deregulates mitochondria and inhibits tumor growth in MYCN-amplified Neuroblastoma

Luca Montemurro[1*], Salvatore Raieli[2*], Silvia Angelucci[1], Damiano Bartolucci[1], Camilla Amadesi[2], Silvia Lampis[2], Anna Lisa Scardovi[2], Leonardo Venturelli[2], Giammario Nieddu[2], Lucia Cerisoli[2], Matthias Fischer[3], Gabriella Teti[4], Mirella Falconi[4], Andrea Pession[1], Patrizia Hrelia[5], Roberto Tonelli[5]

[1]Interdepartmental Center for Cancer Research, University of Bologna, Bologna, Italy. [2]R&D Department, BIOGENERA SpA, Bologna, Italy. [3]Department of Experimental Pediatric Oncology, University Children's Hospital of Cologne, Medical Faculty, Cologne, Germany; and Center for Molecular Medicine Cologne (CMMC), University of Cologne, Cologne, Germany. [4]Department of Biomedical and Neuromotor Sciences-DBNS, University of Bologna, Bologna, Italy. [5]Department of Pharmacy and Biotechnologies, University of Bologna, Bologna, Italy.

* These authors equally contributed to the work

Running title: New MYCN antigene causes mitochondrial deregulation in MNA-NB

Keywords: neuroblastoma, MYCN, antigene oligonucleotide, mitochondria, mitophagy.

Additional information

Financial support: R. Tonelli, A. Pession, P. Hrelia are funded by University of Bologna. G. Teti and M. Falconi are funded by University of Bologna (Ricerca fondamentale orientata - RFO 2017, 2018) and by Fondazione del Monte di Bologna e Ravenna. L. Montemurro, S. Angelucci, and D. Bartolucci are funded by AGEOP. S. Raieli, C. Amadesi, S. Lampis, A. Scardovi, G. Nieddu, and L. Cerisoli are funded by Biogenera SpA.

Corresponding Author: Roberto Tonelli, Department of Pharmacy and Biotechnologies, University of Bologna, Irnerio Street 48, 40126 Bologna, Italy. Phone: +39-051-209-1784; E-mail: roberto.tonelli@unibo.it

Disclosure of Potential Conflicts of Interest: R. Tonelli and A. Pession are BIOGENERA shareholders and members of the BIOGENERA board. S. Raieli, C. Amadesi, S. Lampis, A. Scardovi, G. Nieddu, and L. Cerisoli are working at BIOGENERA. L. Venturelli is a former BIOGENERA employer. No potential conflicts of interest were disclosed by the other authors.

Others:

Word count: 5082

Figures: 6 (plenary figures), 13 (supplementary figures), Tables (8 supplementary data tables)

Abstract

Approximately half of high-risk neuroblastoma (NB) is characterized by MYCN-amplification. N-Myc promotes tumor progression by inducing cell growth and inhibiting differentiation. MYCN has also been shown to play an active role in mitochondrial metabolism, but this relationship is not well understood. While N-myc is a known driver of the disease, it remains a target for which no therapeutic drug exists. Here, we evaluated a novel MYCN-specific antigene PNA oligonucleotide (BGA002) in MYCN-amplified (MNA) or MYCN-expressing NB, and investigated the mechanism of its anti-tumor activity. MYCN mRNA and cell viability were reduced in a broad set of NB cell lines following BGA002 treatment. Furthermore, BGA002 decreased N-myc protein levels and apoptosis in MNA-NB. Analysis of gene expression data from neuroblastoma patients revealed that MYCN was associated with increased reactive oxygen species (ROS), downregulated mitophagy and poor prognosis. Inhibition of MYCN caused profound mitochondrial damage in MNA-NB cells through downregulation of the mitochondrial molecular chaperone TRAP1, which subsequently increased ROS. Correspondigly, inhibition of MYCN reactivated mitophagy. Systemic administration of BGA002 downregulated N-myc and TRAP1 with a concomitant decrease in MNA-NB xenograft tumor weight. In conclusion, this study highlights the role of N-myc in blocking mitophagy in NB and in conferring protection to ROS in mitochondria through upregulation of TRAP1. BGA002 is a potently improved MYCN-specific antigene oligonucleotide that reverts N-myc dysregulated mitochondrial pathways, leading to loss of the protective effect of N-myc against mitochondrial ROS.

Significance:

A second generation antigene peptide oligonucleotide targeting MYCN induces mitochondrial damage and inhibits growth of MYCN-amplified neuroblastoma cells.

Introduction

Neuroblastoma (NB) is the deadliest pediatric tumor. While patients with a low or intermediate risk have a favorable outcome, the high-risk group has a survival rate below 50% (1). The latter group often presents with MYCN amplification (50% of the high risk group) (2). N-Myc is a well-known driver of the disease (3) and is strongly associated with poor survival prognosis (4,5). N-Myc promotes cell growth, inhibits cell differentiation while maintaining a stem-like phenotype; its levels correlate with metastasis and the induction of angiogenesis (6,7). Furthermore, MYCN over-expression affects metabolism to support the higher energy demand of the tumor cells (8–10). Beyond increasing glycolysis and glutaminolysis, N-Myc is involved in mitochondrial functional alteration, however, the mechanism of this effect is not fully understood (11).

Interestingly, MYCN is expressed during embryogenesis and is virtually absent during adulthood (12). All these factors make N-Myc a promising target for neuroblastoma therapy. However, in order for an inhibitor to be effective, it should either interfere with the N-Myc/MAX heterodimers, or with N-Myc interaction with DNA, without inhibiting the highly homologous myc. These requirements have led to N-Myc being currently considered an unlikely target for therapeutic intervention (13).

Although indirect therapeutic approaches in combating neuroblastoma by inhibiting N-Myc have been proposed, considering the broad role of MYCN in neuroblastoma and the lack of a complete understanding of its mechanism, the challenge still remains. Given the difficulties encountered in developing a small molecule inhibitor, other approaches including the use of oligonucleotides, have been tested to inhibit the MYC family (14,15). Differing from the use of antisense oligonucleotides, which inhibit mRNA translation, the antigene approach involves binding to chromosomal DNA, resulting in the inhibition of transcription. By persistently blocking transcription, the antigene oligonucleotides showed higher efficacy compared to antisense oligonucleotides (14–17). Furthermore, PNAs demonstrated potent and specific antigene activity (14–17) and higher therapeutic potential due to their resistance to nuclease degradation (18).

In the present work we show for the first time that BGA002, a new and highly improved antigene PNA oligonucleotide, can specifically target a unique sequence on the MYCN gene. We also demonstrate a new mechanism for the inhibition of MYCN, and ultimately confirm the efficacy of BGA002 *in vivo.*

Materials and Methods

Cell lines. All the cell lines used in this study were obtained during the 2018. Cell lines were obtained from DSMZ (KELLY, LAN5, CHP-134, SiMa, MHH-NB11, NGP, LS, NMB, LAN-1, LAN-6, LAN-2, NBL-S), ECACC (SK−N−DZ, SK-N-F1, NB69), ATCC (HEK293) and kindly gifted by Gaslini Institute, Genova (GI-LI-N, SMS-KAN), by Professor Paolucci G. (SJ-N-KP), Professor Della Valle G (IMR32, SK-N-BE(2)-C, TET-21N) and by professor Spampinato SM (SH-SY5Y). All cell lines are stored in liquid nitrogen and kept in culture for a maximum of 30 days and less than 7 passages from the time they are obtained. The average number of passages for each cell line used in this study is 3. Cell line authentication was not conducted. Cell lines were verified to be negative for the presence of *Mycoplasma* every 3 months by a PCR-based method with the kit LookOut Mycoplasma PCR Detection Kit (Sigma Aldrich) using the manufacturer's instructions. The list of cell lines used in this study with additional details is available as part of the supplementary materials (Supplementary Table 1).

Cell line treatment. BGA001 and BGA002 were produced by Biogenera. PNA-peptide was either available, stored at -20°C, and ready for use, or freshly produced by the Chemistry department and delivered to the Biology department after purification and dilution. PNA was designed and prepared according to previously published studies (16,17). Cell lines were expanded in RPMI 1640, with 10% fetal bovine serum (FBS). Adherent cells were detached with PBS-EDTA, collected, washed, and centrifuged. Cells were counted and resuspended in OPTIMEM. For PNA-peptide treatment (BGA001 and BGA002), 50000 cells were plated in a 24-well flat-bottom plate for RNA extraction, 5000 cells were plated in a 96-well flat-bottom plate for cell viability assays. Cell lines were treated with increasing concentrations (range: 0.08 µM to a maximum of 20 µM) of PNA-peptide. Small interfering RNA (siRNA) for MYCN (sense: UGAUGAAGAGGAAGAUGAAtt, antisense: UUCAUCUUCCUCUUCAUCAtt), TRAP1 (S179, Thermo Fisher Scientific) were mixed with Lipofectamine (Invitrogen) and then diluted in OPTIMEM. Fifty thousand cells were plated in a 24 well plate and incubated with siRNA (100 nM MYCN siRNA, 50 nM *TRAP1* siRNA). After 6 hours of treatment, 4 % FBS was added to the cells.

Quantitive real-time PCR. After 12 hours, the cell lines were detached with PBS-EDTA, centrifuged, and transferred to a 1.5 mL eppendorf tube. The pellet was lysed and stored at -20 °C. RNA was extracted using the RNAspin Mini RNA isolation Kit (GE Healthcare). Prior to use, each sample of RNA was quantified with the Nanodrop spectrophotometer (Thermo Fisher Scientific). One hundred ng of RNA was resuspended for each sample. Retrotranscription and real-time PCR was performed as previously described (17). The list of primers in this study is listed in Supplementary Table 2. Crossing points (Cp) from each analyte were

120 calculated using the second derivative maximum method, and the expression level was quantified by
121 comparison to the BIRC4 gene.
122
123 **Cell viability assay.** Four technical replicates were prepared for each experiment. After 72 hours of
124 treatment, the cells were treated according to the CellTiter-Glo Luminescent Cell Viability Assay protocol
125 (Promega). Luminescence was recorded with the Infinite F200 instrument (Tecan). The percentage of the
126 effect was calculated based on mean luminescence of the control.
127
128 **Western blot.** Cell were lysed 24 hours post treatment in sample lysing buffer (RIPA buffer (150 mM NaCl,
129 1.0% IGEPAL® CA-630, 0.5% sodium deoxycholate, 0.1% SDS, 50 mM Tris, pH 8.0) with Halt protease
130 inhibitor cocktail (Thermo Fisher Scientific). For N-Myc staining, the pellet was resuspended in sample
131 lysing solution on ice (about 50 µL for 5x10 5 cells), and homogenized with a probe sonicator on ice. For
132 OPTN, TRAP1, and, cytochrome c staining, mitochondria were isolated from cultured cells as previously
133 described (19). Total protein extract was quantified using the BCA method with NanoDrop ND-1000
134 spectrophotometer against a standard curve of BSA in sample lysing solution. Ten to thirty µg of protein
135 was mixed with Bolt® Sample Reducing Agent (10X), and Bolt® LDS Sample Buffer (4X) (both from Thermo
136 Fisher Scientific). The samples were then denatured and loaded with SeeBlue® Plus2 Pre-stained Protein
137 Standard and SuperSignal® Enhanced Molecular Weight Protein Ladder onto a Polyacrylamide Bolt® Bis-Tris
138 Plus Gel and run with Bolt® MES SDS Running Buffer (20X). The gel transfer was conducted with the iBlot™
139 Gel Transfer System. Five percent dry milk in PBS-Tween (1X PBS, 0.1% Tween-20) was used as the blocking
140 solution. The membrane was incubated with the following antibodies: N-Myc (SCsc-53993, Santa Cruz), B-
141 Tubulin (SC-9104, Santa Cruz), OPTN (sc-166576C2, Santa Cruz), TRAP1 (sc-13557TR1, Santa Cruz), and
142 Cytochrome C (sc-13156A8, Santa Cruz) diluted in 3.5% BSA, PBS-0.1% Tween-20. The secondary antibody
143 used was anti-mouse antibody (SCsc-2031 HRP, Santa Cruz). Super Signal® West Pico was used as the HRP
144 substrate.
145
146 **Apoptosis analysis.** Kelly cell lines were treated as described above. The Tet21N cells were cultured with or
147 without tetracycline for at least 72 hours and were then detached, washed, and stained with annexin V / PI
148 (ROCHE) according to the manufacturer's instructions. The cell samples were analyzed by the CytoFLEX
149 flow cytometer (Beckman Coulter). The data were analyzed with FlowJo software (Tree Star).
150
151 **Mitochondrial net analysis.** Kelly (60.000 cells) were seeded on 12x12mm circular glass in a 24-well plate
152 for 24 hours in Optimem medium, treated with 5 µM BGA002 or 50 nM TRAP1 siRNA with the addition of
153 4% FBS 6 hours post treatment. At the end of the treatment, MitoTracker® Deep RedFM (M22426; Thermo
154 Fisher Scientific) was added according to the manufacturer's instructions. Cells were fixed with 4% PFA and

were mounted on a glass slide with SlowFade ™ Diamond Antifade Mountant (S36967; Thermo Fisher Scientific). Images were acquired with a confocal microscope (Leica TCS LS). ImageJ was used to capture the images. Briefly, the signal was reduced with a subtraction command with a value of 25 and the images were convolved with a Gaussian blur (σ =1)

Transmission electron microscopy. Kelly cells were seeded onto a 24x24 mm square glass support in a 6-well plate overnight. PNA oligo treatment was performed as described above. Tet21N cells, cultured for at least 72 hours with or without tetracycline, were seeded as described above, and treated overnight with 60 µM chloroquine (vesicular blocking) (20). After 24 hours, fixative solution (2.5% glutaraldehyde in cacodylate buffer 0.1M pH 7.4) was added for 2 hours. The samples were then stored in cacodylate buffer at 4°C. Cells were then post fixed with a solution of 1% osmium tetroxide in 0.1 M cacodylate buffer and embedded in epoxy resins after a graded-acetone serial dehydration step. Ultrathin slices of 100 nm were stained by uranyl acetate solution and lead citrate, and then analyzed by a transmission electron microscope, CM10 Philips (FEI Company) at an accelerating voltage of 80 kV. Images were recorded with a Megaview III digital camera (FEI Company).

Bioinformatic analysis. Neuroblastoma arrays were downloaded (E-MTAB-1781) and normalized. Briefly, mitochondrial involved genes were selected from GO and the literature and used to train a self-organizing map and to cluster patient gene expression profiles. Survival and differential expression gene analyses were applied on the two found clusters. A self-organizing map and random forest model were used to perform feature selection to build a score. ClueGO application was used to find pathway enrichment networks differentially present in the two clusters. The genes in the ROS and Mitophagy pathway lists were obtained from the ClueGO analysis. A detailed description was presented for the bioinformatic data in the extended materials and methods (supplementary files).

ROS measurement. Kelly and Tet21N cell lines were seeded as described above. After 48 hours, the glass support on which the cells were cultured were stained with 2',7'-dichlorofluorescin diacetate (DCFDA) (Sigma-Aldrich) and MitoSOX™ Red Mitochondrial Superoxide Indicator (M36008, ThermoFisher) according to the manufacturer's instructions. Cell were fixed as described above and analyzed by confocal microscopy. The acquired data were processed by the ImageJ processing program. Kelly cells were treated as described above, detached, stained with DCFDA, and subjected to flow cytometry with the CytoFLEX cytometer (Beckman Coulter) for ROS quantification. Data were analyzed using FlowJo software.

Neuroblastoma luminescent cells. Phoenix-Ampho cells were transfected with Lipofectamine 2000 (Invitrogen) and plasmid pMMP-Lucneo (kindly provided by Professor Andrew Kung, Harvard Medical

School, Boston, MA). The viral particles were collected at 48 and 72 hours post transfection. The Kelly cell line was spinoculated with the viral particles and polybrene (hexadimethrine bromide, Sigma). The cells were subjected to selection for 15 days with 1 mg/mL of G418 (Calbiochem). The best cell clones were selected and their luminescence was measured. The resulting cell line was named Kelly-*luc*.

Xenograft ectopic neuroblastoma mouse model. All experiments were approved by the Scientific Ethical Committee of Bologna University (protocol n. 07/73/2013 and 564/2018-PR). Four to six week old NOD/SCID CB17 mice of both sex were inoculated with $10x10^6$ Kelly-*luc* cells in Corning®Matrigel® Matrix. Mice were sedated with isoflurane prior to the injection. The pellet was inoculated by injection in the dorso-posterior-lateral position. The growth of the tumor was evaluated by luminescence acquisition. D-Luciferine was administered by I.P. injection. Luminescence was acquired by the UviTec imaging system (Uvitec, Cambridge, UK). Treatment was performed after the tumor reached the pre-defined starting point in the bioluminescent acquisition. PNA oligo was then administered to the treatment group every day for 14 days. The animals were sacrificed at day fifteen. The tumors were removed, measured, weighed, and fixed in 4% formalin. For the event free survival curve, mice were treated daily with a dorsal subcutaneous injection of 100 μL of vehicle or BGA002 (10 mg/kg/day) for 28 days. Animals were monitored once every other day for tumor diameter measurement (using a caliper) and total tumor volume was extrapolated. An endpoint of at least 10mm tumor diameter and a total tumor volume of $523mm^3$ was established.

Immunohistochemistry. The neuroblastoma tumors were dehydrated, embedded in paraffin, and cut into 4 μm sections. Paraffin removal was accomplished by incubating histological slides in toluene followed by incubation in ethanol. The slides were incubated in 2% H_2O_2-methanol for inhibition of endogenous peroxidase activity. Hydration was performed by serial incubation with 96% ethanol, 70% ethanol, and distilled water. Antigen retrieval was performed by heat processing in 1mM EDTA, pH 8, for N-Myc antibody and in 10mM Citrate pH 6 for TRAP1. The slides were blocked with 10% BSA in PBS, stained with the N-Myc (OP13, Calbiochem), Ki-67 (MIB1, Dako), and TRAP1 (TR1, Santa Cruz) antibodies and subsequently treated with secondary antibody (anti-mouse, Dako). The peroxidase coloration reaction was performed using the Dako DAB kit. The slides were stained with haematoxylin, dehydrated, and mounted. Images were acquired with the Leitz Diaplan microscope.

Statistical analysis. Statistical analysis was performed with the Prism software version 6 (GraphPad) or with R software version 3.5. Python software version 3.0 was used to perform t-SNE. The different analyses and tests were specifically designed for each experiment.

Results

BGA002 is a novel MYCN-specific antigene oligonucleotide with potently improved MYCN transcriptional inhibition

We have previously reported on the effect of a MYCN-specific antigene PNA (agPNA) oligonucleotide (BGA001) for the selective inhibition of MYCN in NB cell lines. This inhibition led to decreased transcription, reduced cell viability, and apoptosis (16). Furthermore, the MYCN agPNA was able to inhibit MYCN transcription in rhabdomyosarcoma cell lines, which led to anti-tumor activity *in vivo* in mice (17). Thus, our first aim was to compare the effects of the novel MYCN-specific agPNA oligonucleotide (BGA002) with the previous one (BGA001). BGA002 was conjugated to a nuclear localization signal (NLS) peptide for delivery (16,21,22), because it was previously found to facilitate penetration of BGA001 into cells, without requiring a transfection agent, and localization to the nucleus. Indeed, BGA002 showed potently enhanced activity in down-regulating MYCN mRNA expression in comparison with the agPNA BGA001 in MNA-NB cells (Fig. 1A). Moreover, BGA002 was much more efficient in reducing cell viability and N-Myc protein degradation than BGA001 (Fig. 1B and 1C), and in inducing apoptosis at 24 and 48 hours (Fig. 1D and S1A). Therefore, as demonstrated by the EC_{50} comparison, BGA002 shows a stronger anti-tumor effect *in vitro* in comparison with the previous agPNA (Supplementary Table 3).

To evaluate the *in vitro* activity of BGA002 in NB, we selected a panel of twenty cell lines to cover the broad landscape of NB tumors: MNA cell lines (n = 10), MNA/$p53_{mut}$ (n = 4), not-MNA (n = 5), and not-MNA/$p53_{mut}$ (n = 1). All the selected NB cell lines, showed expression of MYCN mRNA, with consistently higher levels detected in MNA cell lines (Fig. S2A). BGA002 shows a strong dose-dependent inhibitory effect on MYCN transcription and on cell viability (Fig. 1E and F, S2B and D). MNA cell lines were significantly more susceptible to the effects of BGA002 as demonstrated by a lower EC_{50} compared to the MNA/$p53_{mut}$ cell line (Fig. 1F).

As expected, BGA002 was MYCN-specific, and did not influence cell viability in the MYCN-unexpressed HEK293 cells (Fig. S3A), while a mutated version of BGA002 ($BGA002_{mut}$) did not have any effect on MYCN transcription (Fig. S3B), on cell viability of MYCN-expressing MNA-NB cells (Fig. S3C), on N-Myc downstream targets (Fig. S3D), and on inducing apoptosis (Fig. S3E-F). Moreover, BGA002 bound to the unique target DNA sequence in the MYCN gene, while $BGA002_{mut}$ showed no binding (Fig. S3G).

Specific MYCN-inhibition by BGA002 leads to profound mitochondrial damage in MNA-NB cells

Since MYCN mRNA inhibition persisted at 48 hours (Fig. S2C), at which time we found extensive apoptosis levels (Fig. 1D), we decided to perform transmission electron microscopy to investigate the leading cause of this phenomenon. Ultrastructural analysis showed that MYCN inhibition by BGA002 caused profound

mitochondrial changes in MNA-NB cells. After 12 hours, we observed initial mitochondrial damage (Fig. S4A) without concomitant apoptosis (Fig. S4B and C), suggesting that apoptosis is a consequence of the observed phenomenon, rather than the cause. After 48 hours (or 72 hours) of BGA002 treatment, the mitochondria had sustained extensive damage (Fig. 2A, Fig. S5C) while at 24 hours we noticed that mitochondria became smaller and the cristae patterns were much less elaborate (Fig. S5B). Indeed, mitochondrial alterations were not observed after treatment with a mutated control antigene PNA ($BGA002_{mut}$), after 48 hours or at 72 hours (Fig. S5A and C).

Generally the distribution and connection pattern is indicative of mitochondrial mass and function (23,24). While Mito-Tracker staining reveals that in the untreated MNA-NB cells the mitochondria are highly interconnected, anti-MYCN BGA002 treatment disrupted these mitochondrial nets, and the mitochondrial content appears to be reduced (Fig. 2B and S5D). Moreover, BGA002 induced a change in the mitochondrial pattern, resulting in a perinuclear distribution (Fig. 2B). As before, $BGA002_{mut}$ failed to affect the mitochondrial nets (Fig. S5D). Interestingly, we observed much less mitochondrial damage and pattern alteration after 48 hours of BGA001 (Fig. S6A-B). Furthermore, BGA002 treatment led to a decrease in mitochondrial area per cell (25) in the MNA cells (Fig. S7A), and we observed a BGA002 dose-dependent mitochondrial mass reduction after 48 and 72 hours of treatment (Fig. S7B-C).

Alterations in mitochondrial pathways can identify neuroblastoma patients with poor survival prognosis

To verify the impact of mitochondrial gene signature on neuroblastoma prognosis we selected genes from the GO mitochondrial pathways and from the available literature (1718 genes, Supplementary Table 4). For this purpose we used a publicly available dataset that included patient clinical annotations (26). We used the mitochondrial related signature to conduct a self-organization map to separate gene expression profiles from NB in two different clusters of patients (Fig. 3A-C, S8A, Supplementary Table 5). The two clusters have a statistically significant difference in the overall survival rates and event-free probability (Fig. 3D, S8B), with cluster 2 strongly linked with a poor survival prognosis. Indeed, cluster 2 shows a similar worsening of the overall survival probability for the MNA patient subgroup (Fig. 3E). We further investigated which genes had a larger effect on event-free and overall survival. For this purpose, we used a random forest model optimized for censored data to conduct feature selection. The variables extracted from the model and from the self-organization map were used to construct a MitoScore. The top 200 genes qualifying for MitoScore are shown in word cloud (Fig. 3F, S8C, Supplementary Table 6). The genes present in MitoScore and differentially expressed in the two clusters (Supplementary Table 7) were used to identify which functional pathways were linked to each cluster. Filtering the insignificant pathways, we found 20 GO pathways specific for cluster 1 and 45 for cluster 2 (Fig. 3G, Supplementary Table 8 and 9). As expected, analysis highlighted the presence of a substantial number of folic acid pathway genes in cluster 2, since it is known

that MYCN amplified neuroblastomas have an enhanced dependency on folate (27). Moreover, cluster 2 contains a number of genes in response to ROS genes (RROS) (Fig. 3G, Supplementary Table 9). Conversely, we found that cluster 1 contained a significant number of genes related to mitophagy (Fig. 3G, Supplementary Table 9). Based on pathway analysis we built an RROS score and a mitophagy score. The high presence of genes related to response to ROS was significantly predictive for overall survival. It was also noted that that a lower number of genes present related to mitophagy significantly worsened the overall survival probability (Fig. 3H). The RROS and mitophagy scores showed significant inverse correlation (Pearson coefficient = -0.73, pvalue = 2.2e-16). Interestingly, the presence of MYCN correlated well with the RROS score (0.63, pvalue = 2.2e-15) and showed inverse correlation with the mitophagy score (-0.73, pvalue = 2.2e-16) (Fig. S8E). Ultimately, it was noted that the results from MYCN-amplified patients showed a substantial presence of mitochondrial related signature genes and a higher RROS score in comparison with patients lacking MYCN-amplification (Fig S9A)

BGA002 reverts N-Myc dysregulated mitochondrial pathways in MNA-NB

MYCN alteration of the transcriptional program is critical in promoting tumorigenesis in MNA-NB. Given this view, we investigated the effects of MYCN inhibition by BGA002 on gene expression profiles in several NB cell lines. As expected, genes present in the mitochondrial signature, and with a high score, show different expression levels between cluster 1 and cluster 2 (Fig. 4A). Surprisingly, we found the same behavior in MYCN-amplified versus MYCN non-amplified patients (Fig. 4A). Furthermore, we noticed that these genes are significantly predictive for overall survival (Fig. 4B). We also found that different genes in the mitochondrial signature correlate well or show inverse correlation with MYCN in the dataset of patient gene expression profiles (Fig. 4C). Based on these results, we investigated if MYCN inhibition by BGA002 was able to down-regulate genes from the mitochondrial signature (Fig. 4D). MYCN inhibition led to the down-regulation of a wide group of mitochondrial genes in the different NB cell lines. MYCN silencing by BGA002 also down-regulated other previously described MYCN-related genes (Fig. 4D), including TERT and SKP2 (28,29). The use of an anti-MYCN siRNA and the Tet21N cells (in which inducible MYCN silencing is achieved by tetracycline administration, but not by BGA002, since these cells lack the agPNA target sequence in the inserted MYCN construct (Fig. S10A)(30) as controls, resulted in the same gene expression pattern (Fig. 4D). Interestingly, by confirming MYCN correlation with a response to ROS and an inverse correlation with mitophagy as previously shown, we found that MYCN-inhibition down-regulated the gene expression of TRAP1 while up-regulating the expression of OPTN (Fig. 4D). These genes are involved in mitochondrial ROS control and in mitophagy, respectively (31–33). We also confirmed mitochondrial protein production variation in MNA-NB cells, a concomitant decrease in TRAP1, and an increase in OPTN production (Fig. 4E). Moreover, TRAP1 decrease and OPTN increase are accentuated at 48 hours (Fig. 4E).

Based on our finding that MYCN shows inverse correlation with the mitophagy score in NB and on the well described important positive role of OPTN in this pathway (32), we investigated the inhibitory role of MYCN on mitophagy activation. In Tet21N cells after MYCN-silencing (72 hours of tetracycline administration) while not observing apoptosis, (Fig. S10B and C), we registered a dramatic decrease in mitochondrial number (Fig. S10D). Concomitantly, we observed the appearance of a high number of myelin figures (Fig. 4F) and co-localization of mitochondria with lysosomes (Fig.S10E). Collectively, these findings are indicative of mitophagy activity after MYCN inhibition. Finally, an siRNA anti-OPTN significantly reduced mitophagy activity after MYCN silencing in Tet21N cells (Fig. S11A-D)

BGA002 leads to loss of protective N-Myc effect against mitochondrial ROS through TRAP1 downregulation in MNA-NB

Based on our finding of a positive correlation between MYCN expression and the RROS score in the poor survival prognosis cluster 2 from the NB patient dataset (Fig. S8E), we investigated if MYCN inhibition by BGA002 could induce augmentation of mitochondrial ROS production. Indeed, BGA002 treatment induced up-regulation of the ROS and an increase in superoxide production (Fig. 5A, S12A). Since TRAP1 plays a determining role in mitochondrial ROS control and considering that BGA002 treatment down-regulated *TRAP1* expression, we investigated if TRAP1 inhibition led to an increment in ROS production in MNA-NB. Indeed, siRNA against TRAP1 (siTRAP1) led to an increment in production of ROS in mitochondria (Fig. 5A). TRAP1 downregulation by siTRAP1 also inhibited the mitochondrial net structure (Fig. 5B), similar to MYCN inhibition after BGA002 treatment. Moreover, siTRAP1 consistently reduced cell viability (Fig. 5C). As a control, we verified that siTRAP1 did not affect MYCN mRNA expression (Fig. 5D). Interestingly, in Tet21n cells, which showed mitophagy reactivation after MYCN silencing (by tetracycline administration) and did not undergo apoptosis, we did not find an appreciable increase in ROS production (Fig. S12B). Moreover, $BGA002_{mut}$ failed to induce ROS production, while BGA001 showed a modest effect (Fig. S12C) and the latter did not consistently reduce TRAP1 mRNA expression (Fig. S12D). This mechanism is graphically represented in Fig. S13A.

BGA002 causes elimination of MNA-NB in mice

Finally, we evaluated the *in vivo* anti-tumor activity of BGA002 in a xenograft murine model of MNA-NB. We inoculated MNA-NB Kelly-luminescent cells, which were monitored until tumor luminescence was detectable. Treatment with BGA002 resulted in a statistically significant augmentation of survival in comparison with the vehicle (Fig. 6A, S13B).

Moreover, subcutaneous administration (daily for 15 days) of BGA002 resulted in a potent and dose-dependent anti-tumor activity. BGA002 at 2.5 mg/kg/day caused a tumor weight decrease of 25%, while the treatment with 5 mg/kg/day resulted in a significant decrease of more than 70%, and administration at 10 mg/kg/day led to tumor elimination (Fig. 6B). We concluded that treatment with BGA002 showed a dose-response tumor growth inhibition.

After treatment with BGA002 at the intermediate dose (5 mg/kg/day), histological analysis revealed a consistent reduction in tumor vascularization as compared to the vehicle group (Fig. 6C), while immunohistochemical analysis, showed a consistent reduction in N-Myc protein staining, a decrease in Ki-67, leading to reduced TRAP1 protein expression (Fig. 6C).

Discussion

The critical role of N-Myc in cancer development and its association with poor survival prognosis is not restricted to neuroblastoma, with a broad range of tumors available in which MYCN-amplification and over-expression play a crucial role (34). Due to the highly restricted pattern of expression of MYCN in normal cells, N-Myc represents an optimal target for tumor-specific therapy for MYCN-expressing tumors.

While the direct targeting of the N-Myc transcription factor protein is still challenging, antigene therapy by targeting MYCN transcription has great potential in treating MYCN-expressing tumors, as we previously demonstrated in the preclinical treatment of neuroblastoma and rhabdomyosarcoma by a MYCN-specific antigene PNA (16,17).

Here we report for the first time, the preclinical results for BGA002, a novel MYCN-specific agPNA with potently improved ability to block MYCN transcription. The BGA002 sequence is complementary to a unique target sequence in the human (and mouse) MYCN gene. BGA002 showed dose-dependent inhibition of MYCN transcription and cell viability in a panel of twenty MYCN-expressing NB cell lines with or without MNA. In comparison to BGA001, it showed a potently enhanced ability to specifically decrease MYCN mRNA and protein expression while decreasing the viability of NB cell lines.

Interestingly, BGA002 is more effective in NB cell lines with MNA versus p53-mutated or MYCN single copy cell lines. Since, MYCN inhibition led to apoptosis, the higher EC_{50} found in p53-mutated NB cells could be explained by their higher resistance to apoptosis (35). MYCN inhibition led to the down- or up-regulation of highly relevant genes involved in metabolism, cell cycle control, apoptosis, metastasis, and DNA repair.

Surprisingly, the main ultrastructural alteration that we found in MNA-NB cells after MYCN inhibition, was alteration of mitochondrial structure and organization. Interestingly, BGA001, which showed much less ability to induce mitochondrial alteration, exerted a lesser effect in the promotion of apoptosis. We also showed that a gene expression signature related to mitochondria allows for the identification of neuroblastoma patients with poor survival prognosis. Furthermore, we found that BGA002 treatment led to the down- or up-regulation of different genes involved in this signature.

It is known that metabolic stress generally leads to autophagy (36), but its role in cancer is still controversial (37,38). The impact of autophagy in neuroblastoma is also controversial (39) and depends on the p53 status of the cells (40). Moreover, mitophagy (a particular type of autophagy) is a fundamental process for mitochondrial turnover and health, and its deregulation can result in neurodegenerative disease and cancer insurgence (41,42). Interestingly, we found that low enrichment in mitophagy related genes is significantly predictive for a poor survival prognosis in a large dataset of gene expression profiles from NB patients. Furthermore, we noticed that MYCN inhibition led to the up-regulation of OPTN, which plays an important role in mitophagy induction (32,33). Moreover, blocking MYCN expression in Tet21N cells led to the disappearance of mitochondria with concomitant presence of myelin figures, and co-localization of

lysosomes with mitochondria, indicating mitophagy activation. This phenotype is significantly reduced after siRNA anti-OPTN administration, indicating that N-Myc blocks mitophagy through OPTN silencing.

ROS generation in mitochondria plays a role in cancer initiation, with many mitochondrial processes leading to ROS generation in tumor cells (43). Notwithstanding their role in tumorigenesis, ROS excess in cells leads to damage and ultimately to apoptosis (44). TRAP1 is a mitochondrial chaperone protein that plays a crucial role in mitochondrial homeostasis (31), and its down-regulation corresponds to an increase in ROS presence, and to a higher susceptibility to oxidative stress (31). We found that inhibition of MYCN led to TRAP1 down-regulation, an increase ROS generation, and induction of apoptosis in MNA-NB cells. Furthermore, BGA001 modestly reduced TRAP1 expression and showed a less effective ability to induce ROS and promote apoptosis, indicating that N-Myc mitochondrial protection plays a relevant role in neuroblastoma.

There is a growing corpus of evidence that mitochondrial fate is connected to tumor formation and progression (45,46). Neuroblastoma insurgence leads to profound metabolic changes, where high risk neuroblastoma shows a higher uptake of glucose and a reduction in oxidative phosphorylation in mitochondria (47). Although it has been claimed that N-Myc was involved in mitochondrial lipid metabolism in NB (11), its role in mitochondrial regulation in NB was largely unknown.

Here, we describe for the first time that N-Myc is relevant in mitochondrial structural maintenance and turnover. Our work highlights the prognostic value of mitochondrial dysregulation in NB patients and provides a mechanism on how N-Myc controls previously unknown aspects of mitochondrial function, by inhibiting mitophagy, and controlling ROS generation.

Considering the role of N-Myc in a wide range of tumors, further studies on its close relationship with mitochondria will provide other valuable insights in cancer biology. Furthermore, considering the role of MYCN in mitochondrial ROS protection, it will be interesting to analyze the potential use of BGA002 in conjunction with other therapies that induce ROS in cancer cells.

BGA002 has received orphan drug designation from the Food and Drug Administration (orphan registry: DRU-2017-6085) and from the European Medicines Agency (orphan registry: EU/3/12/1016). Based upon its well tolerated regulatory safety profile package, BGA002 is now moving to phase I clinical trials in Neuroblastoma patients.

Acknowledgments

We would like to thank Wissem Eljeder and Simone Maestri for suggestions and comments. We would like also to thank Andres E. Zucchetti from the Institut Curie for insightful suggestions on confocal microscopy analysis.

References

1. Pinto NR, Applebaum MA, Volchenboum SL, Matthay KK, London WB, Ambros PF, et al. Advances in Risk Classification and Treatment Strategies for Neuroblastoma. J Clin Oncol. 2015;33:3008–17.

2. Campbell K, Gastier-Foster JM, Mann M, Naranjo AH, Van Ryn C, Bagatell R, et al. Association of MYCN copy number with clinical features, tumor biology, and outcomes in neuroblastoma: A report from the Children's Oncology Group. Cancer. 2017;123:4224–35.

3. Weiss WA, Aldape K, Mohapatra G, Feuerstein BG, Bishop JM. Targeted expression of MYCN causes neuroblastoma in transgenic mice. EMBO J. 1997;16:2985–95.

4. Brodeur GM, Seeger RC, Schwab M, Varmus HE, Bishop JM. Amplification of N-myc in untreated human neuroblastomas correlates with advanced disease stage. Science. 1984;224:1121–4.

5. Seeger RC, Brodeur GM, Sather H, Dalton A, Siegel SE, Wong KY, et al. Association of multiple copies of the N-myc oncogene with rapid progression of neuroblastomas. N Engl J Med. 1985;313:1111–6.

6. Huang M, Weiss WA. Neuroblastoma and MYCN. Cold Spring Harb Perspect Med. 2013;3.

7. Matthay KK, Maris JM, Schleiermacher G, Nakagawara A, Mackall CL, Diller L, et al. Neuroblastoma. Nat Rev Dis Primer. 2016;2:16078.

8. Dang CV, Kim J, Gao P, Yustein J. The interplay between MYC and HIF in cancer. Nat Rev Cancer. 2008;8:51–6.

9. Qing G, Li B, Vu A, Skuli N, Walton ZE, Liu X, et al. ATF4 Regulates MYC-mediated Neuroblastoma Cell Death upon Glutamine Deprivation. Cancer Cell. 2012;22:631–44.

10. Ruiz-Pérez MV, Henley AB, Arsenian-Henriksson M. The MYCN Protein in Health and Disease. Genes. 2017;8.

11. Zirath H, Frenzel A, Oliynyk G, Segerström L, Westermark UK, Larsson K, et al. MYC inhibition induces metabolic changes leading to accumulation of lipid droplets in tumor cells. Proc Natl Acad Sci U S A. 2013;110:10258–63.

12. Zimmerman KA, Yancopoulos GD, Collum RG, Smith RK, Kohl NE, Denis KA, et al. Differential expression of myc family genes during murine development. Nature. 1986;319:780–3.

13. Fletcher JI, Ziegler DS, Trahair TN, Marshall GM, Haber M, Norris MD. Too many targets, not enough patients: rethinking neuroblastoma clinical trials. Nat Rev Cancer. 2018;18:389–400.

14. Janowski BA, Kaihatsu K, Huffman KE, Schwartz JC, Ram R, Hardy D, et al. Inhibiting transcription of chromosomal DNA with antigene peptide nucleic acids. Nat Chem Biol. 2005;1:210–5.

15. Janowski BA, Huffman KE, Schwartz JC, Ram R, Hardy D, Shames DS, et al. Inhibiting gene expression at transcription start sites in chromosomal DNA with antigene RNAs. Nat Chem Biol. 2005;1:216–22.

16. Tonelli R, Purgato S, Camerin C, Fronza R, Bologna F, Alboresi S, et al. Anti-gene peptide nucleic acid specifically inhibits MYCN expression in human neuroblastoma cells leading to cell growth inhibition and apoptosis. Mol Cancer Ther. 2005;4:779–86.

17. Tonelli R, McIntyre A, Camerin C, Walters ZS, Leo KD, Selfe J, et al. Antitumor Activity of Sustained N-Myc Reduction in Rhabdomyosarcomas and Transcriptional Block by Antigene Therapy. Clin Cancer Res. 2012;18:796–807.

18. Nielsen PE, Egholm M, Berg RH, Buchardt O. Sequence-selective recognition of DNA by strand displacement with a thymine-substituted polyamide. Science. 1991;254:1497–500.

19. Clayton DA, Shadel GS. Isolation of Mitochondria from Tissue Culture Cells. Cold Spring Harb Protoc. 2014;2014:pdb.prot080002.

20. Dolman NJ, Chambers KM, Mandavilli B, Batchelor RH, Janes MS. Tools and techniques to measure mitophagy using fluorescence microscopy. Autophagy. 2013;9:1653–62.

21. Boffa LC, Cutrona G, Cilli M, Matis S, Damonte G, Mariani MR, et al. Inhibition of Burkitt's lymphoma cells growth in SCID mice by a PNA specific for a regulatory sequence of the translocated c-*myc*. Cancer Gene Ther. 2007;14:220–6.

22. Cutrona G, Carpaneto EM, Ulivi M, Roncella S, Landt O, Ferrarini M, et al. Effects in live cells of a c-*myc* anti-gene PNA linked to a nuclear localization signal. Nat Biotechnol. 2000;18:300–3.

23. Detmer SA, Chan DC. Functions and dysfunctions of mitochondrial dynamics. Nat Rev Mol Cell Biol. 2007;8:870–9.

24. Sauvanet C, Duvezin-Caubet S, di Rago J-P, Rojo M. Energetic requirements and bioenergetic modulation of mitochondrial morphology and dynamics. Semin Cell Dev Biol. 2010;21:558–65.

25. Vowinckel J, Hartl J, Butler R, Ralser M. MitoLoc: A method for the simultaneous quantification of mitochondrial network morphology and membrane potential in single cells. Mitochondrion. 2015;24:77–86.

26. Oberthuer A, Juraeva D, Hero B, Volland R, Sterz C, Schmidt R, et al. Revised Risk Estimation and Treatment Stratification of Low- and Intermediate-Risk Neuroblastoma Patients by Integrating Clinical and Molecular Prognostic Markers. Clin Cancer Res. 2015;21:1904–15.

27. Lau DT, Flemming CL, Gherardi S, Perini G, Oberthuer A, Fischer M, et al. MYCN amplification confers enhanced folate dependence and methotrexate sensitivity in neuroblastoma. Oncotarget. 2015;6:15510–23.

28. Evans L, Chen L, Milazzo G, Gherardi S, Perini G, Willmore E, et al. SKP2 is a direct transcriptional target of MYCN and a potential therapeutic target in neuroblastoma. Cancer Lett. 2015;363:37–45.

29. Nikiforov MA, Chandriani S, Park J, Kotenko I, Matheos D, Johnsson A, et al. TRRAP-Dependent and TRRAP-Independent Transcriptional Activation by Myc Family Oncoproteins. Mol Cell Biol. 2002;22:5054–63.

30. Wasylishen AR, Stojanova A, Oliveri S, Rust AC, Schimmer AD, Penn LZ. New model systems provide insights into Myc-induced transformation. Oncogene. 2011;30:3727–34.

31. Masgras I, Sanchez-Martin C, Colombo G, Rasola A. The Chaperone TRAP1 As a Modulator of the Mitochondrial Adaptations in Cancer Cells. Front Oncol. 2017;7.

32. Moore AS, Holzbaur ELF. Dynamic recruitment and activation of ALS-associated TBK1 with its target optineurin are required for efficient mitophagy. Proc Natl Acad Sci U S A. 2016;113:E3349–58.

33. Richter B, Sliter DA, Herhaus L, Stolz A, Wang C, Beli P, et al. Phosphorylation of OPTN by TBK1 enhances its binding to Ub chains and promotes selective autophagy of damaged mitochondria. Proc Natl Acad Sci U S A. 2016;113:4039–44.

34. Rickman DS, Schulte JH, Eilers M. The Expanding World of N-MYC–Driven Tumors. Cancer Discov. 2018;8:150–63.

35. Chesler L, Goldenberg DD, Collins R, Grimmer M, Kim GE, Tihan T, et al. Chemotherapy-Induced Apoptosis in a Transgenic Model of Neuroblastoma Proceeds Through p53 Induction. Neoplasia N Y N. 2008;10:1268–74.

36. Dikic I, Elazar Z. Mechanism and medical implications of mammalian autophagy. Nat Rev Mol Cell Biol. 2018;19:349–64.

37. Rybstein MD, Bravo-San Pedro JM, Kroemer G, Galluzzi L. The autophagic network and cancer. Nat Cell Biol. 2018;20:243–51.

38. Wilde L, Tanson K, Curry J, Martinez-Outschoorn U. Autophagy in cancer: a complex relationship. Biochem J. 2018;475:1939–54.

39. Frentzel J, Sorrentino D, Giuriato S. Targeting Autophagy in ALK-Associated Cancers. Cancers. 2017;9.

40. Mrakovcic M, Fröhlich LF. p53-Mediated Molecular Control of Autophagy in Tumor Cells. Biomolecules. 2018;8.

41. Bordi M, Nazio F, Campello S. The Close Interconnection between Mitochondrial Dynamics and Mitophagy in Cancer. Front Oncol. 2017;7.

42. Palikaras K, Lionaki E, Tavernarakis N. Mechanisms of mitophagy in cellular homeostasis, physiology and pathology. Nat Cell Biol. 2018;20:1013–22.

43. Sabharwal SS, Schumacker PT. Mitochondrial ROS in cancer: initiators, amplifiers or an Achilles' heel? Nat Rev Cancer. 2014;14:709–21.

44. Murphy MP, Holmgren A, Larsson N-G, Halliwell B, Chang CJ, Kalyanaraman B, et al. Unravelling the Biological Roles of Reactive Oxygen Species. Cell Metab. 2011;13:361–6.

45. Sciacovelli M, Gonçalves E, Isaac Johnson T, Roberto Zecchini V, da Costa ASH, Gaude E, et al. Fumarate is an epigenetic modifier that elicits epithelial-to-mesenchymal transition. Nature. 2016;537:544–7.

46. Vyas S, Zaganjor E, Haigis MC. Mitochondria and Cancer. Cell. 2016;166:555–66.

47. Aminzadeh S, Vidali S, Sperl W, Kofler B, Feichtinger RG. Energy metabolism in neuroblastoma and Wilms tumor. Transl Pediatr. 2015;4:20–32.

Figure legends

Figure 1.

BGA002 is a new specific anti-MYCN antigene oligonucleotide with potently improved MYCN transcription inhibition properties leading to cell-growth inhibition and apoptosis in Neuroblastoma cells.
A – E, Comparison of the *in vitro* efficacy between neuroblastoma cells (Kelly and SK-N-BE(2)c) treated with different doses of BGA001 and BGA002. Bars represent the mean, whiskers indicate standard deviation. **A,** MYCN mRNA expression inhibition through RT-PCR after 12 hours of treatment, BGA001 (gray) and BGA002 (red) (n = 3, biological replicates for each cell line). **B,** Cell viability assay showing a decrease after 72 hours of treatment, BGA001 (gray) and BGA002 (red) (n = 3, biological replicates for each cell-line). **C,** Representative western blot analysis of N-Myc after 24 hours. Representative staining for N-Myc (above) and whole-lane coomassie staining are presented (bottom). Quantification of N-Myc expression (normalized with coomassie staining) is presented in the top panel. Bars represent the mean, whiskers indicate standard deviation (n = 2, biological replicates for each cell line). BGA001 is shown on the left, and BGA002 on the right, Kelly cell line is shown in the first line, SK-N-BE(2)c is shown in the second line. **D,** the bar represents percentage of cells stained by Annexin V^+ / PI^+ for the cell line treated for 24 (left) or 48 hours (right) (n = 3, biological replicates for each cell-line). **E,** Heatmap representing different neuroblastoma cell lines treated with different doses of BGA002. MYCN mRNA expression inhibition through RT-PCR (left) after 12 hours of treatment and a decrease in cell viability after 72 hours of treatment (right). The red scale represents the average percentage of inhibition of different biological replicates for each cell line (n = 3) normalized to the control. **F,** mRNA MYCN inhibition (left) and vitality decrement (right) EC_{50} for each cell line grouped according to MYCN amplification and/or p53 mutation. Each dot represents a singular experiment (n = 3 for each cell-line). Each point represents an individual sample, middle line indicates the median, box limits indicate the first and third quartiles, the whiskers indicate samples within 1.5 times the interquartile range (test = Wilcoxon matched pair test. pValue: *, $p < 0.05$, **, $p < 0.01$, ***, $p < 0.001$).

Figure 2.

BGA002 leads to MYCN-specific structural and functional alterations in mitochondria in MNA-NB cells.
A, Transmission electron micrographs of the Kelly cell line treated for 48 hours with 5 µM BGA002. Untreated cells are shown in the first row, BGA002 treated cells are shown in the second row. Abbreviations used: M: mitochondrion, N: nucleus. **B,** Evaluation of mitochondrial nets in the Kelly cell line treated for 48 hours with 5 µM BGA002.

Figure 3.

Alterations in mitochondrial pathways identify neuroblastoma patients with poor survival prognosis.

A, Schematic representation of the bioinformatic pipeline analysis conducted. A dataset of neuroblastoma gene expression profiles (GEP) has been downloaded. Genes selected from the literature or listed in GO as part of the mitochondrial associated terms were used to generate a mitochondrial related signature. A self-organization map (SOM) was utilized to associate patient GEPs to two different clusters with a different survival probability. The genes in the mitochondrial related signature were ranked by their contribution to the separation of patient GEPs in two different clusters. Their contributions to predicting overall survival and event-free survival were also taken into account to build a MitoScore for all the genes present in the mitochondrial related signature. We used genes in the MitoScore that were differentially expressed to build a functional grouped network of pathways. **B,** Heatmap showing the two different clusters (cluster1 in green, cluster2 in red) derived from the self-organization map. Each square represents a neuron; the size of the inner square is proportional to the number of patient GEPs associated with that neuron. **C,** T-distributed stochastic neighbor embedding showing the clustering of the transcriptional profiles (considering the genes present in the mitochondrial related signature) of the patient GEPs. Each dot represents a patient transcriptional profile, the dots are colored according to which cluster they belong to (cluster1 (n = 541) in green, cluster2 (n= 122) in red). **D,** Kaplan–Meier plots for the probability of overall survival over time for patients associated with cluster 1 (green, n = 541) and cluster 2 (red, n = 161). Associated P value (log-rank test) is shown in the middle. Hazard ratio and associated P value (log-rank test) are shown in the bottom left of the plot. **E,** Kaplan–Meier plots for the probability of overall survival over time for patients associated with cluster 1 (green) and cluster 2 (red), MNA patient (light red, n = 122) and non-MNA patient (light green, n = 580). **F,** Word cloud of the top 200 genes ranked by MitoScore, the size is proportional to the associated MitoScore. **G,** Functional grouped network of the pathways up-regulated in cluster 1 (in green) and cluster 2 (in red). Circle size is proportional to the P value (FDR < 0.05). **H,** Kaplan–Meier plots for the probability of overall survival over time for patients associated with Response to ROS score (low enriched, n = 614, high enriched, n = 88, top panel) and Mitophagy score (low enriched, n = 73, high enriched, n = 629, bottom panel). P value associated with the curve is shown in the middle of the plot (log-rank test). Hazard ratio and associated P value (log-rank test) are shown in the bottom left of the plot. (*, $p < 0.05$, **, $p < 0.01$, ***, $p < 0.001$)

Figure 4.

Blocking of MYCN leads to MYCN-specific gene expression signature inhibition in NB cells and to mitophagy reactivation.

A, Expression of different genes presented in the mitochondrial related signature in cluster 2, cluster 1, MNA and non-MNA patient gene expression profiles and presented as z-scores. Each point represents an individual sample, middle line indicates the median, the whiskers indicate samples within 1.5 times the

638 interquartile range (statistical test = Wilcoxon). **B,** Kaplan–Meier plots for the probability of overall survival
639 over time for patients associated with different genes present in the mitochondrial related signature. For
640 NME4, TRAP1, MRPL11, PPRC1, MRPS2 the dark gray line represents a z-score > 1, for OPTN a z-score < -1.
641 Hazard ratio, p value (log-rank test) are shown in the bottom left of the plot. **C-D,** the gene names in the
642 middle refer to both panels. **C,** the color scale represents Pearson's correlation coefficient of genes present
643 in the mitochondrial related signature (top) and other N-Myc targets (bottom) with MYCN in the patient
644 GEP dataset. **D,** Heatmap of the gene expression variation in neuroblastoma cell lines (MNA, MNA/p53-
645 mut, non-MNA, non-MNA/ p53-mut) after 12 hours of BGA002 treatment (5 µM). On the right side of the
646 heatmap, Kelly cells treated with anti-MYCN siRNA, and Tet21N cells treated with tetracycline (72 hours)
647 are shown. The color scale represents the $\log_2$ fold change in comparison to the untreated cell line (n = 2
648 for each cell line), gray (gene not expressed). Upper part: genes present in the mitochondrial related
649 signature, bottom part: other N-Myc targets. **E,** Western blot analysis for TRAP1 (left, top row) and OPTN
650 (right, top row), cytochrome C (middle row), and coomassie staining (bottom row) of Kelly untreated cells
651 and BGA002 (5 µM) treated cells for 24 (first line) and 48 hours (second line). **F,** Transmission electron
652 micrographs of Tet21N cultured cells treated without (first line) and with (second line) tetracycline and
653 chloroquine for 72 hours. From left to right, increasing magnification. Abbreviations used: M:
654 mitochondrion, MF: myelin figure, L: lysosome, N: nucleus. (*, $p < 0.05$, **, $p < 0.01$, ***, $p < 0.001$).
655
656 **Figure 5.**
657 **BGA002 reverts the MYCN control of ROS generation by TRAP1 down-regulation in MNA-NB cells**.
658 **A,** Representative confocal microscopy analysis of ROS production in Kelly untreated cells (first line), Kelly
659 cells treated with 5 µM BGA002 (second line) for 48 hours, Kelly cells treated with anti-TRAP1 siRNA (third
660 line) for 24 hours. Mitosox staining in red (left), DCFDA staining in green (middle), and merge (right). From
661 left to right, increasing magnification. **B,** Evaluation of mitochondrial nets in the Kelly cell line treated for
662 48 hours with vehicle (first line), with 5 µM BGA002 (second line), and 50 nM anti-*TRAP1* siRNA. From left
663 to right, increasing magnification. **C,** Kelly cell line treated with 50 nM siRNA anti-TRAP1. TRAP1 percentage
664 of mRNA inhibition after 24 hours in the left panel, percentage of cell viability inhibition in the right panel
665 (n = 2) after 72 hours. **D,** Kelly cell line treated with 50 nM siRNA anti-TRAP1, TRAP1, and MYCN showing
666 percentage of mRNA inhibition after 24 hours (n= 3).
667
668 **Figure 6.**
669 **BGA002 causes elimination of MNA-NB in mice through TRAP1 down-regulation.**
670 **A,** Kaplan–Meier plots for the probability of event-free survival over time for mice (Kelly-luc xenograft)
671 treated with vehicle (red, n = 6) and BGA002, 10 mg/kg/day (green, n = 8). Associated P value (log-rank test)
672 is shown in the middle. Hazard ratio and associated P value (log-rank test) are shown in the bottom left of

673 the plot. **B,** Evaluation of tumor weight in neuroblastoma xenograft mice treated with different doses of
674 BGA002 (untreated (n=21), 2.5 (n= 11), 5 (n=8), 10 (n=9) mg/kg/day). Each dot represents a mouse (test =
675 Mann Whitney test). The table below the graph indicates the mean value of tumor weight reduction for
676 each treatment dose in comparison to the control. **C,** Immunohistochemical analysis of neuroblastoma
677 xenograft mice untreated (first line) or treated with 5 mg/kg/day BGA002(second line). Images of sections
678 are shown stained with haematoxylin and eosin (first), Ki-67 antibody (second), N-Myc antibody (third), and
679 Trap1 antibody (last). Similar results were obtained from four independent mice. (*, $p < 0.05$, **, $p < 0.01$,
680 ***, $p < 0.001$)
681

Figure 1

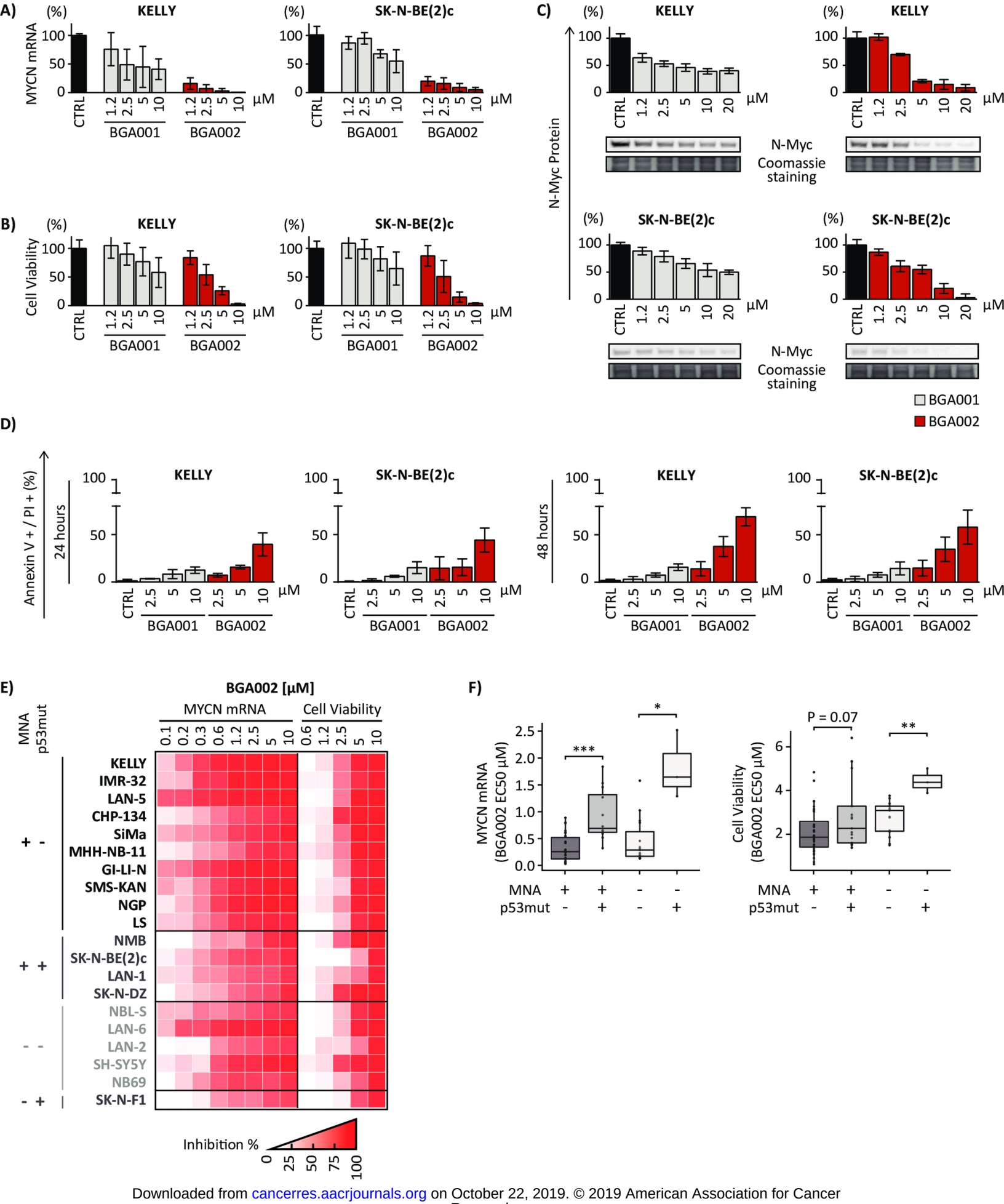

Figure 2

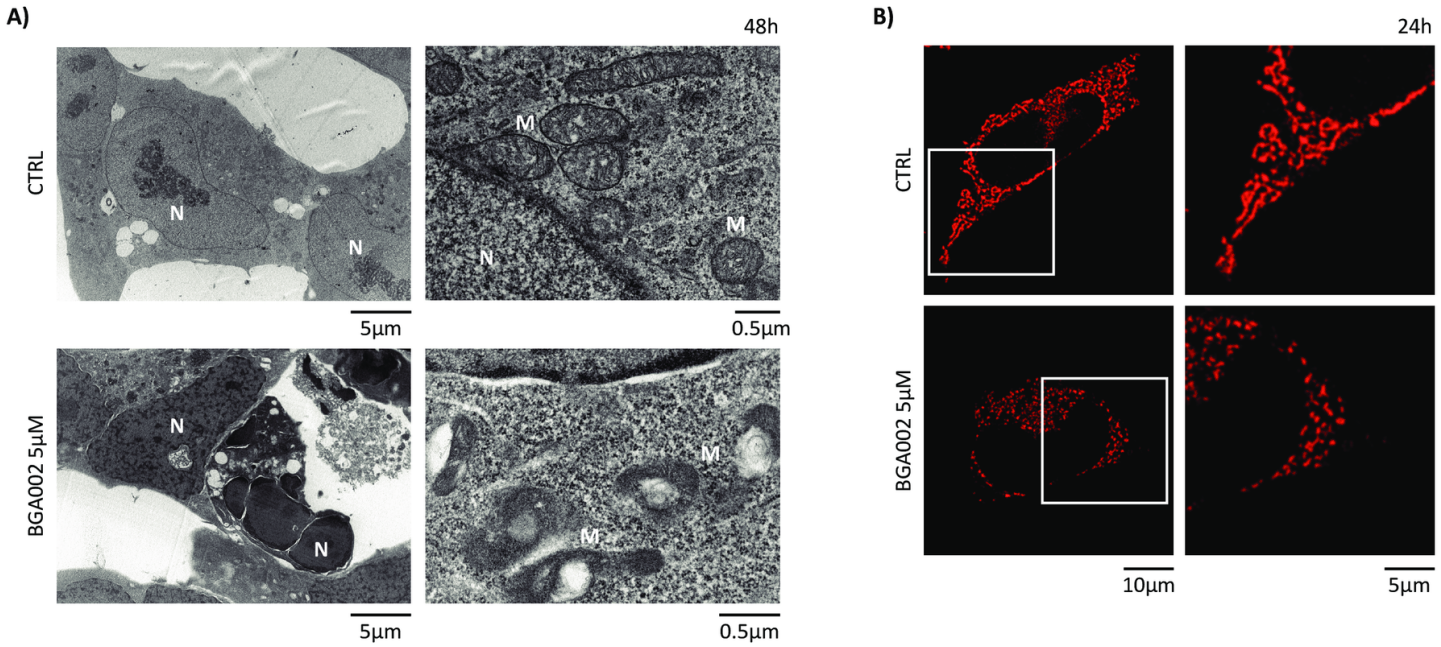

Author Manuscript Published OnlineFirst on October 15, 2019; DOI: 10.1158/0008-5472.CAN-19-0008
Author manuscripts have been peer reviewed and accepted for publication but have not yet been edited.

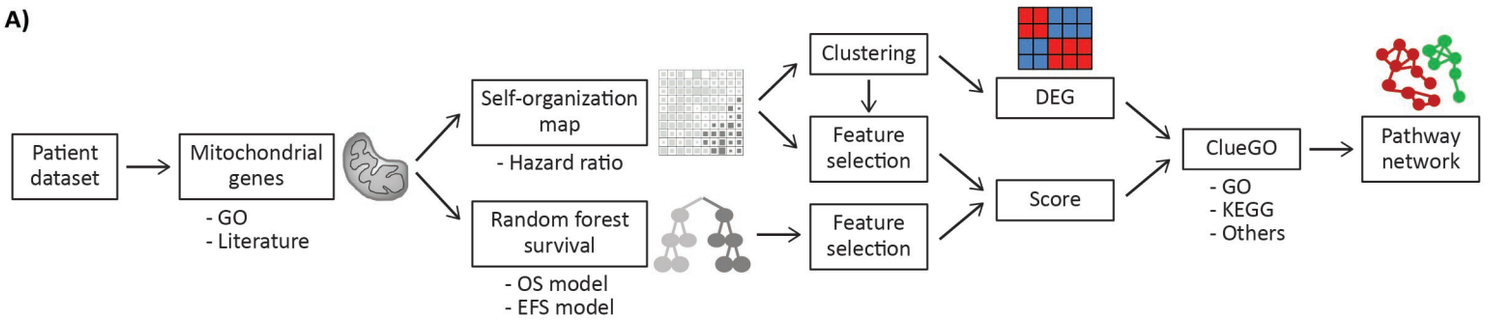

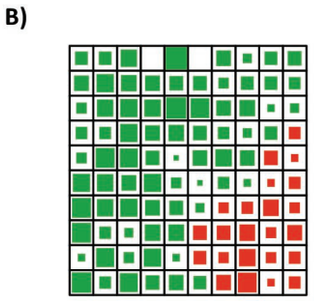

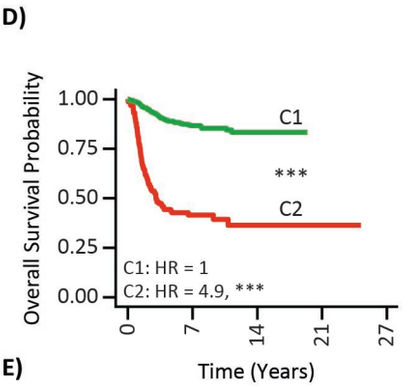

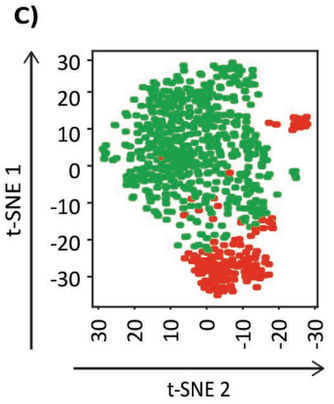

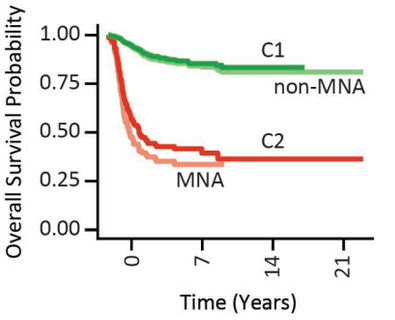

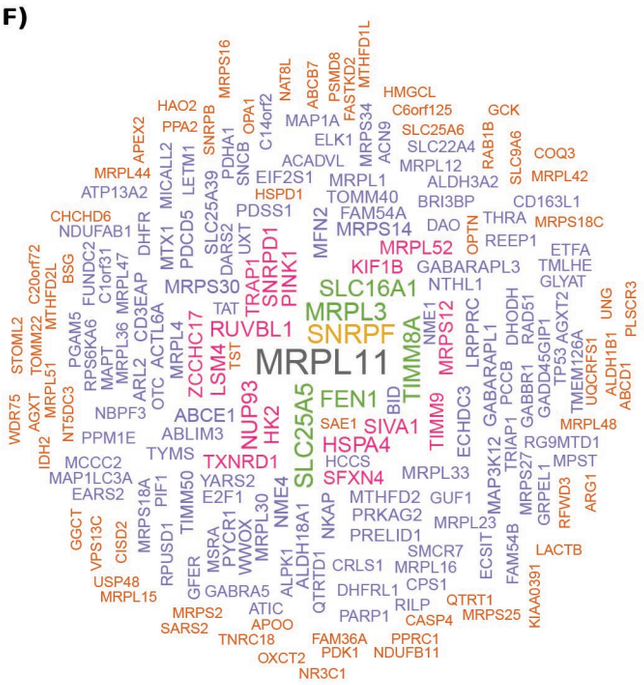

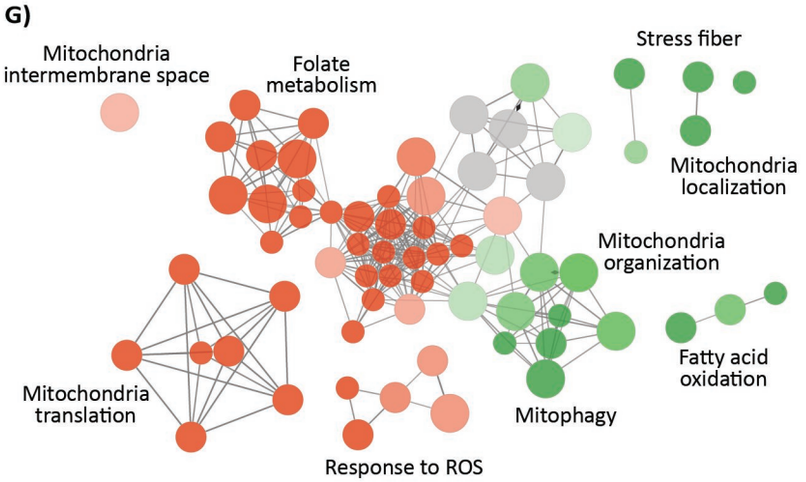

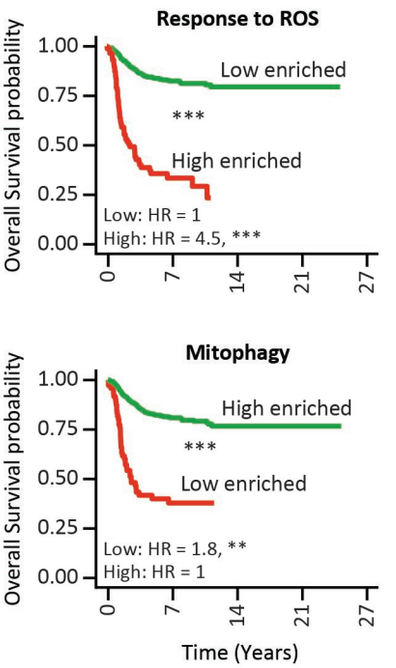

C1 = Cluster 1
C2 = Cluster 2
MNA = MYCN-Amplified
non-MNA = MYCN Non-Amplified

Figure 4

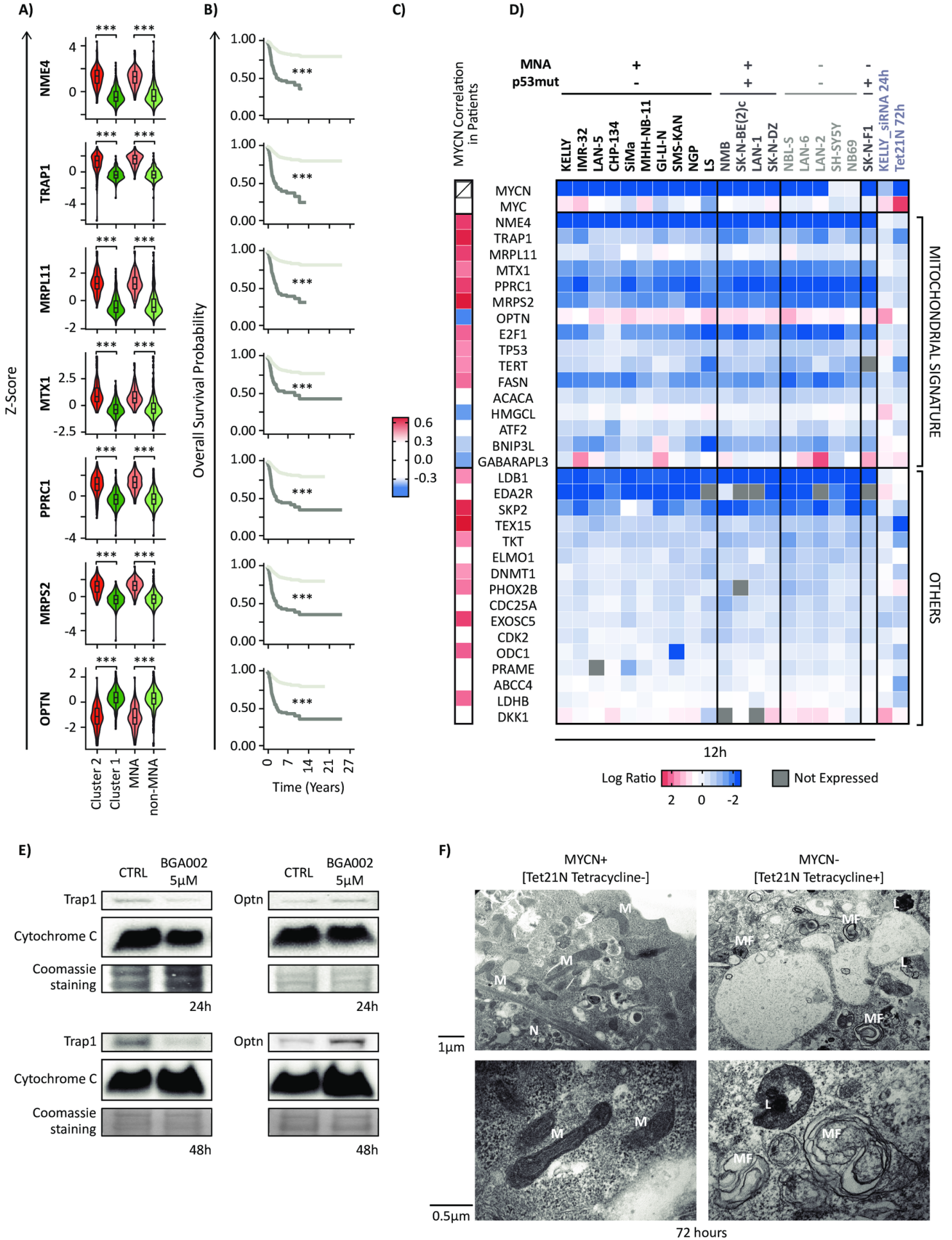

Figure 5

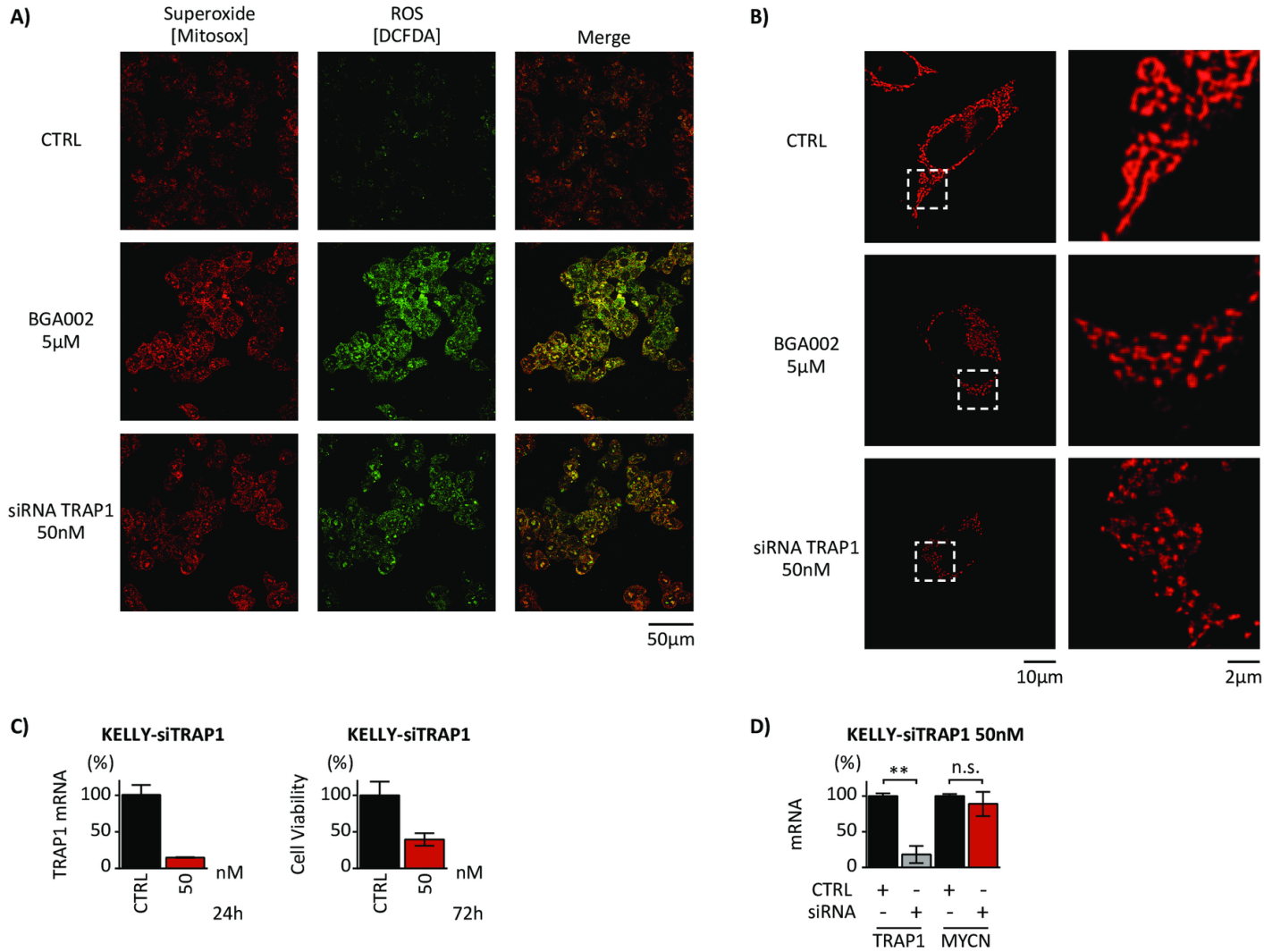

Figure 6

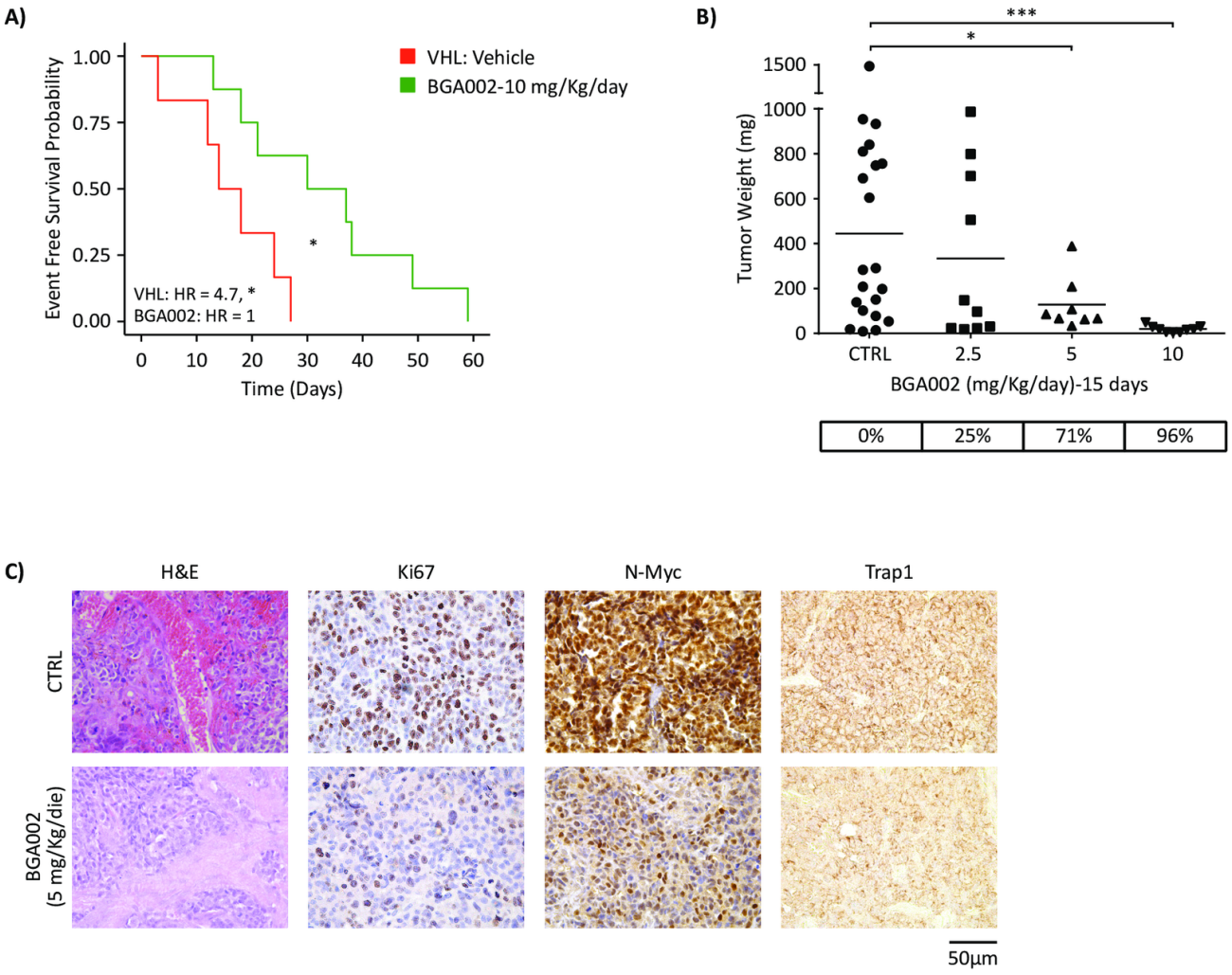

AACR American Association for Cancer Research

Cancer Research

The Journal of Cancer Research (1916–1930) | The American Journal of Cancer (1931–1940)

A novel MYCN-specific antigene oligonucleotide deregulates mitochondria and inhibits tumor growth in MYCN-amplified Neuroblastoma

Luca Montemurro, Salvatore Raieli, Silvia Angelucci, et al.

Cancer Res Published OnlineFirst October 15, 2019.